Nanoindentation of Isotactic Polypropylene: Correlations Between Hardness, Yield Stress, and Modulus on the Local and Global Scales

R. Lesan-Khosh,[1] R. Bagheri,[1] S. Asgari[2]

[1]*Polymeric Materials Research Group, Department of Materials Science and Engineering, Sharif University of Technology, P. O. Box 11155-9466, Tehran, Iran*
[2]*Department of Materials Science and Engineering, Sharif University of Technology, P. O. Box 11155-9466 Tehran, Iran*

Received 16 July 2010; accepted 19 October 2010
DOI 10.1002/app.33635
Published online 25 February 2011 in Wiley Online Library (wileyonlinelibrary.com).

ABSTRACT: The correlations between the hardness, yield stress, and modulus of elasticity of isotactic polypropylene (iPP) were evaluated on the local and global scales. Nanoindentation and traditional macromechanical tests were incorporated for this purpose. Thus, local and global mechanical properties were measured at various temperatures and strain rates. A certain relation was found between the local and global mechanical properties. Moreover, Johnson's model (developed according to the expanding cavity model) was also evaluated at various temperatures and strain rates. The Johnson model was valid only for the yield stresses obtained by nanoindentation and compressive tests and also the elastic modulus obtained via nanoindentation. © 2011 Wiley Periodicals, Inc. J Appl Polym Sci 121: 930–938, 2011

Key words: hardness; indentation; mechanical properties; poly(propylene) (PP)

INTRODUCTION

It is well known that many polymers possess a heterogeneous microstructure, which is induced by the processing conditions. For a semicrystalline polymer, a typical layered arrangement is developed and is normally referred to as a *skin–core microstructure.* The intrinsic molecular nature of the polymer together with the morphology and crystalline structure of these layers determine the mechanical behavior of the polymeric parts. The mechanical characterization of polymeric materials at the microlevel or nanolevel can be important for certain materials selection and design criteria and applications. The indentation test has been used for over 100 years to measure the indentation hardness (H) and other basic mechanical properties of materials on the local scale [e.g., yield stress (Y)].[1] Recent technological advances have permitted us to continuously record the load (P), down to the micro-Newton, and the indentation depth (h), down to a few nanometers, during an indentation test (i.e., nanoindentation). Thus, indentation has gained its reputation and currently is the state-of-the-art technique for determining the local elastic[2] and plastic properties[3,4] of materials. The modulus of elasticity (E),[2,5] Y,[5–8] strain-hardening exponent (n),[7] and viscoelastic properties, that is, creep data,[9] can be extracted from an instrumented indentation test. The nanoindentation test offers several advantages over conventional tension or compression tests, namely, the ability to evaluate local properties, the nondestructive nature of the test, and the small required amount of material required for the test.

To measure E via instrumented indentation, the multiple-point unload method (or Oliver–Pharr method[2]) can be used with the slope of the initial portion of the unloading curve and also the residual h. In general, for a given material, the value of the local modulus of elasticity obtained by the nanoindentation (E_i) is sometimes higher than that measured in conventional tensile or compression tests.[10,11]

The idea of relating the Y values of materials to their H values dates back to the original work of Tabor in 1951.[1] He found that for ductile metals, almost two-thirds of the mean pressure underneath the indenter (p_m) were the hydrostatic component, and therefore, only one-third of that produced plastic flow during indentation. He also showed that for rigid, perfectly plastic materials, H is directly related to Y through the following equation:

$$H = 3\mathrm{Y} \tag{1}$$

Correspondence to: R. Lesan-Khosh (r.lesan@gmail.com).

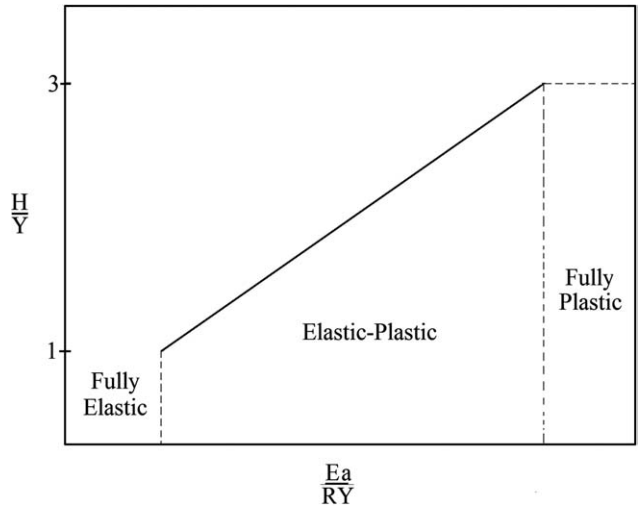

Figure 1 Correlation between H, Y, E, and the indentation geometrical specifications (indentation a/R) in the three regimes of the indentation process.

However, in fact, it has been found that the indentation process can be divided into three distinct regimes: (1) elastic regime, (2) elastic–plastic or transition regime, and (3) plastic regime (Fig. 1).[12] Actually, the fully elastic regime occurred when $p_m/Y \leq 1.07$ (Hertzian theory). Then, yielding commences, and the elastic–plastic transition regime begins with deformation involving both elastic and plastic processes. Plastic deformation starts just underneath the indenter tip and is initially constrained by the surrounding elastic material. Therefore, the constraint factor (C), that is, the ratio of p_m to the representative flow stress ($p_m/\sigma_{(r)}$), increases from 1.07, within the transition regime, to a value of approximately 3. The transition regime ends when the plastic zone breaks through the surface outside the region of contact and the constraint is relieved. In the fully plastic regime, C remains constant at a value of approximately 3.

To this end, theoretical analyses using various models have been proposed to explain the elastic and plastic properties of materials undergoing indentation within the transition regime. Among these models, the expanding cavity model (ECM), developed by Johnson,[13] is particularly valuable. This model is based on Hill's[14] solution for the quasi-static expansion of a spherical shell of an elastic, perfectly plastic material under an internal pressure. With either the Tresca or Von Mises yield criterion, Johnson's spherical cavity model was developed to predict the relationship between H and Y via the following equation:

$$p_m/Y = \mathrm{C} = \mathrm{A} + \mathrm{BlnZ} \tag{2}$$

where A and B are constants and Z is a parameter related to Y/E and the indenter geometry.

Later, with the Drucker–Prager yield criterion, Narasimhan[15] developed a modified ECM to describe the indentation deformation of pressure-dependent materials, as follows:

$$\frac{H}{Y} = \frac{p_m}{Y} = \frac{2}{3}\left[\frac{7}{4} - \frac{\tan\alpha}{3} + \ln\left(\frac{Ea}{4RY}\right)\right] \tag{3}$$

where tan α is the pressure sensitivity index (PSI) of the material, R is the indenter radius and a is radius of contact area. Nevertheless, in this model, the strain-hardening effect was not considered. Recently, Gao, Jing and Subhash[16] developed two new modified ECMs for elastic power-law hardening and linear hardening materials. However, these two new models are confined to pressure-independent materials. For power-law materials, the model can be written as follows:

$$\frac{H}{Y} = \frac{2}{3}\left[\left(1 - \frac{1}{n}\right) + \left(\frac{1}{n} + \frac{3}{4}\right)\left(\frac{Ea}{4RY}\right)^n\right] \tag{4}$$

Considering the concurrent effects of strain-hardening and pressure dependency, Ai and Dai[17] developed a new modified ECM in 2007,[17] which is given as follows (for power-law materials):

$$\frac{H}{Y} = \frac{2}{3}\left[\left(1 - \frac{1}{n}\right)\left(1 - \frac{\tan\alpha}{3}\right) + \left(\frac{1}{n} + \frac{3}{4}\right)\left(\frac{Ea}{4RY}\right)^n\right] \tag{5}$$

In the case of pressure-independent materials, eq. (5) is reduced to eq. (4), and interestingly, for pressure-independent elastic, perfect plastic materials, eq. (4) is reduced to Johnson's model, which is given as follows:

$$\frac{H}{Y} = \frac{2}{3}\left[\frac{7}{4} + \ln\left(\frac{Ea}{4RY}\right)\right] \tag{6}$$

Therefore, from the aforementioned equations, with the required data, Y of the material can be determined by the indentation test.

For polymers, extensive research efforts have been made to find the correlations between H, Y, and E.[18–21] In these studies, in fact, Y and E were obtained by macromechanical tests. Flores et al.[18] showed that H correlates with the tensile yield stress (Y_t) and tensile modulus (E_t) through the following relations:

$$H \cong 3Y_t \tag{7a}$$

$$H \cong E_t/10 \tag{7b}$$

Although the correlation with the compressive yield stress (Y_c) is as follows

$$H \cong 2Y_c \tag{7c}$$

However, some researchers found a different correlation between H and E_t, as follows:[20]

$$H \cong E_t/20 \tag{8}$$

A simple relation between H and Y was found only in the fully plastic regime in the indentation process. Thus, although there is consistency about the existence of a simple relation between H and E_t of a material, the discrepancy is the exact ratio of these two properties.

In addition to the aforementioned phenomenological equations, the relation between Y and E_t of polymers was developed by a model according to the intermolecular forces between two molecules,[21] given as follows:

$$Y_t \cong E_t/30 \tag{9}$$

This relation is consistent with eqs. (7a) and (7b). In fact, the aforementioned investigations deal with the correlations between local measurement (H) and the results of global macromechanical experiments (Y and E_t). However, global macromechanical measurements can be affected by the heterogeneous morphology and crystalline structure of the sample induced by processing conditions. For instance, in the case of an injection-molded sample, the skin and core regions have different mechanical properties. Therefore, traditional tensile and compression experiments give the average bulk mechanical properties of the sample, which can be problematical when compared to local indentation hardness measurements. In fact, one may reprove this correlation between local and global scale measurements. To eliminate this problem, in this study, we dealt with the correlations between local H, Y, and E values. In fact, H, Y, and E were extracted from a nanoindentation process. Further, macromechanical tests were also performed for the comparison of the bulk and local mechanical properties.

EXPERIMENTAL

Material

Commercial-grade isotactic polypropylene (iPP) (melt flow index = 8) was obtained from Imam Khomeini Petrochemical Complex (designated 080) Mahshahr, Iran. Samples were prepared with an injection-molding machine. To produce various skin–core morphologies, the barrel temperature of the apparatus was set at different values (195, 210, 225, and 240°C). The mold temperature was held at about 25°C by water circulation.

Mechanical properties evaluation

Macroscale mechanical properties

To measure Y and E of the bulk samples, tensile and compression tests were carried out at different temperatures (21, 40, 60, and 80°C) and strain rates (10^{-3}, 10^{-2}, and 10^{-1} 1/s). The experiments were performed on an Instron 5567 frame. A heating chamber was used to carry out the tests at elevated temperatures. A precise extensometer was incorporated to determine E_t. The compression tests were conducted in plane strain conditions.

Local mechanical properties

The local elastic and plastic properties of the samples on the microscale were determined by depth-sensing indentation with nanoscale resolution (nanoindentation). The nanoindentation measurements were performed with a fully calibrated UMIS nanoindenter from Commonwealth Scientific and Industrial Research Organisation, Sydney: Australia equipped with precise temperature controls. The displacement and force resolution of the nanoindenter were 0.1 nm and 0.75 μm, respectively. P and h were recorded simultaneously for a complete load–hold–unload cycle with a spherical indenter with a radius (R) of 20 μm. Ten indentations separated by a distance of 25 μm were made on each sample. The indentations were performed on the smooth surface of the cross section of the injection-molded bars. The cross section of the sample was ground by appropriate sand paper and subsequently polished by 0.05-μm alumina powder. The nanoindentation tests were conducted at the range of strain rates and temperatures similar to the tensile and compression tests. The strain rate in nanoindentation was calculated as follows:[22]

$$\dot{\varepsilon} = \frac{\dot{h}}{h} \tag{10}$$

(strain rate)=(displacement rate in depth)/(displacement in depth) E was determined with the Oliver–Pharr method[2] using the following equations:

$$E_r = \frac{\pi}{2(1-\upsilon^2)}\frac{S}{\sqrt{A}} \tag{11a}$$

$$S = \left.\frac{dP}{dh}\right|_{h\max} \tag{11b}$$

where A is the contact area corresponding to the maximum load ($P_{\max}$), S is the stiffness at the inception of the unloading curve, υ is Poisson's ratio, E_r is reduced or effective modulus, and h is indentation depth (see Fig. 2). In the case of a relatively small h,

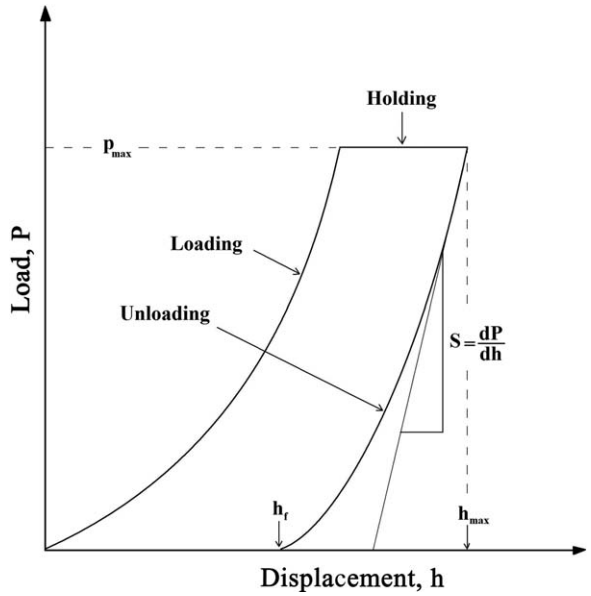

Figure 2 Typical indentation load versus indentation depth curve obtained by the load–hold–unload nanoindentation test.

a spherical indenter can be approximated as a paraboloid of revolution. The contact depth (h_c) is then given by the following equation:

$$h_c = h_{\max} - 0.75\frac{P_{\max}}{S} \tag{12}$$

From geometric considerations, A is

$$A = \pi h_c(2R - h_c) \tag{13}$$

S is affected by the viscoelastic behavior of the material. If the material is creeping under P of the indenter tip and P is suddenly reduced, the displacement may continue to increase even after the applied P is reduced. This behavior creates an abrupt slope change in the unloading curve as the material begins to recover; this makes it difficult to determine the unloading slope. To prevent this, the indenter was held for 60 s after $P_{\max}$ was reached. This time was long enough to mitigate this effect significantly. Thus H and E_i of the samples were calculated through the nanoindentation tests, since $H=P_{max}/A$ and $E_i=E_r$.

The nanoindentation results could also be used to extract Y of the materials on the local scale. For this purpose, as mentioned in the Introduction, the analytical equations developed for the transition regime were applied. With the values of PSI and n of polypropylene (PP), the yield stress by nanoindentation (Y_{ECM}) can be obtained from Eq. 5. Actually, the it could be considered an ideal elastic–plastic material up to strian $\varepsilon \approx 10\%$. After this amount of strain, it exhibited strain-hardening behavior (see Fig. 3). It

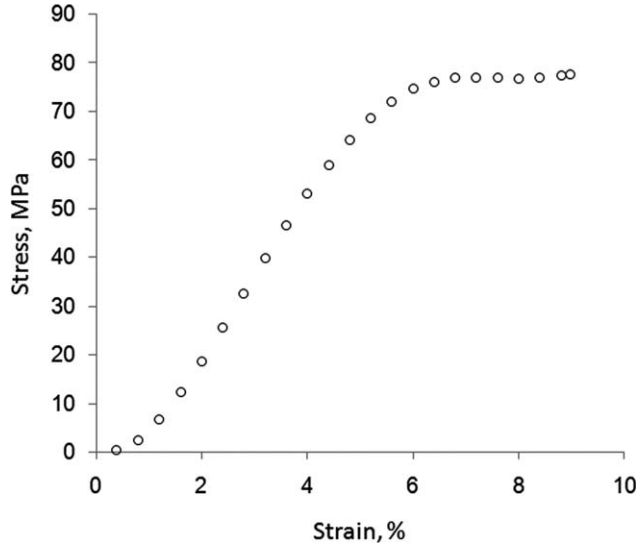

Figure 3 Compression stress–strain curve for a PP sample.

should be pointed out that For a spherical indenter, the strain in indentation ($\varepsilon_{indentation}$) is calculated as follows:[6]

$$\varepsilon_{\text{indentation}} \approx \frac{0.2a}{R} \approx \varepsilon_r \tag{14}$$

where ε_r is the representative strain in the macromechanical test. However, in this study, the maximum representative strain was about 7%. Therefore, the n value in eq. (5) could be neglected. In other words, eq. (3) could be used to extract Y via the indentation test.

Figure 4 illustrates the effect of the pressure sensitivity of the material in the elastic–plastic regime of

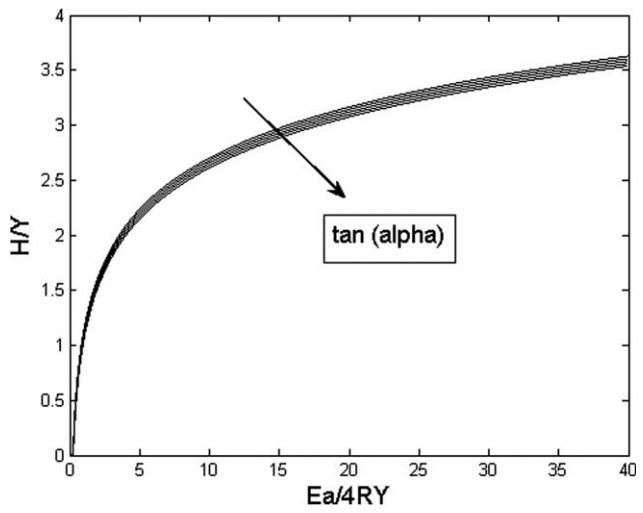

Figure 4 Effect of pressure dependency of the material on the elastic–plastic regime of indentation (tan α varied from 0 to 0.5).

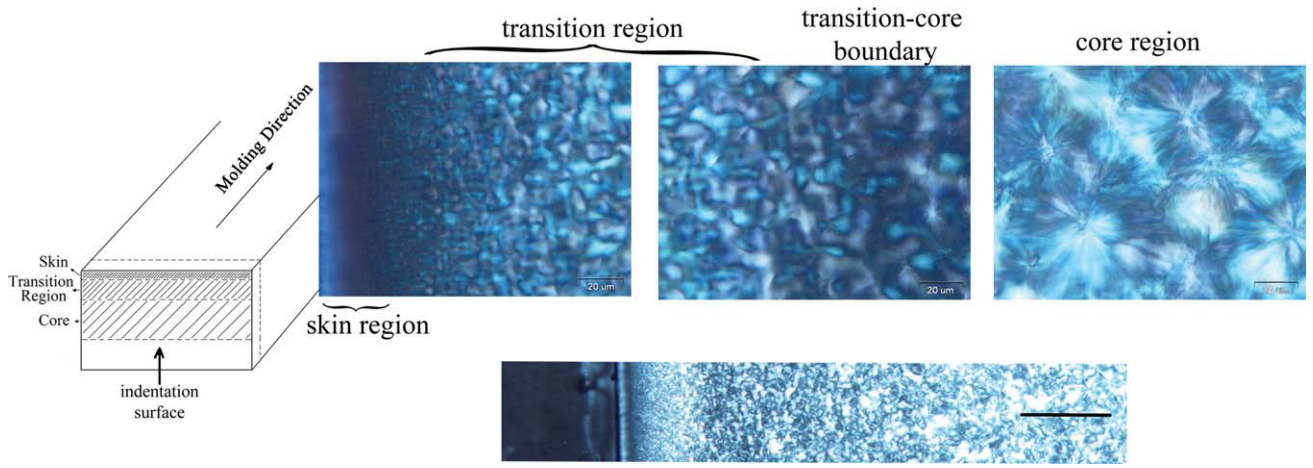

Figure 5 TOM of the skin–core structure of the injection-molded PP. [Color figure can be viewed in the online issue, which is available at wileyonlinelibrary.com.]

the indentation. As shown, changing tan α from 0 to 0.5 did not induce any significant changes in the indentation response. Therefore, to measure Y_{ECM}, the PSI value could also be ignored. Thus, Johnson model, that is eq.6, could be used to extract Y_{ECM}.

Microscopy

To study the skin–core structure of the injection-molded samples, transmission optical microscopy TOM; Olympus BX52 (Tokyo,: Japan) was incorporated. Thin slices (50–100 μm) perpendicular to the molding direction were prepared via polishing (see schematic in Fig. 5).

RESULTS AND DISCUSSION

Local versus global mechanical properties

Figure 5 illustrates the skin–core morphology of an injection-molded PP. As seen, three distinct regions, that is, the skin, transition, and core, were recognized. The local mechanical properties of each individual layer and also the average global mechanical properties of the bulk sample are plotted in Figure 6. As illustrated, E_i and Y_{ECM} showed progressive increase from the skin to the core. In fact, depending on the crystalline structure and morphology, each layer had specific mechanical properties. However, only an average mechanical property can be given for the bulk sample. Figure 6(b) also compares the Y values of the samples obtained by various macroscale methods. As shown, the magnitude of the local Y value obtained at the core region was almost equal to Y_c. This may have been due to the fact that in the compression experiment, the core region had the most influence on the mechanical properties of the sample compared to the skin and transition regions, that is, the edge of the sample.

Figure 7 compares the effect of changing the melting temperature of iPP during the injection-molding process on the microstructure of the samples. Clearly, the skin thickness decreased with increasing melting temperature. Larger spherulite size was also found in samples processed at a higher melting

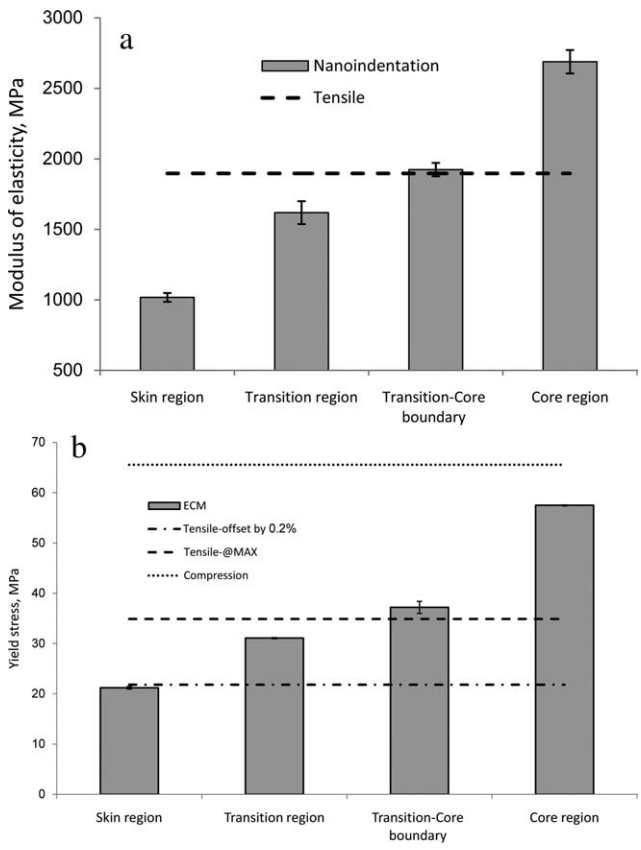

Figure 6 Plots of (a) E and (b) Y, of the injection-molded PP samples on the local and global scales.

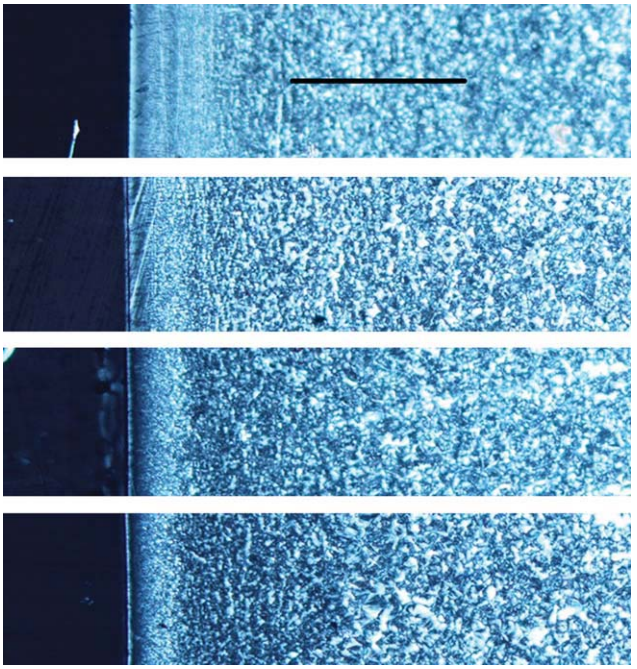

Figure 7 TOM of the injection-molded samples processed at different melting temperatures (T_m's). [Color figure can be viewed in the online issue, which is available at wileyonlinelibrary.com.]

temperature. The effect of altering the melting temperature on the local- and global mechanical properties of the iPP samples are also summarized in Figure 8(a,b). The local mechanical properties with increasing melting temperature in all of the layers close to the skin. This behavior may have been due to the fact that with increasing melting temperature, the crystalline orientation and also formation of cylindrical crystallites were eliminated.[23] However, E_i and Y_{ECM} increased with increasing melting temperature at the core region. This may have been due to the increase in the spherulite size (as evident in Fig. 7) and also the increase in the degree of crystallinity.[23] As shown in Figure 8, whereas an increase in the melting temperature led to decreases in E_i and Y close to the skin, it did not change E_t and Y on the global scale. As illustrated in Figure 8(a), E_i of all of the samples at the core was always greater than E_t. Actually, there was an almost constant difference (ca. 500 MPa) between them. Obviously, the reduction of the plastic region size beneath the indenter tip led to a more precise measurement of E_i and, consequently, the observation of closer E_i and E_t values. To create this condition, h into the sample had to be minimized. In the case of a spherical indenter, this means that the ratio of the indentation depth to the radius of the indenter tip (h/R) was kept as low as allowed. However, to have better accuracy in the local Y measurement larger plastic deformation is preferred. Thus, in this study, all nanoindentation tests were carried out in at an h/R equal 0.06.

The local (core region) and global mechanical properties of PP are summarized in Table I. As also shown in Figure 8(b), in general, Y_{ECM} for the core was very close to the global Y_c. Obviously, during the indentation process, the stress state beneath the indentation tip was compressive. Therefore, this agreement between Y_{ECM} and Y_c was expected. For the rest of this study, the local mechanical tests were only carried out at the core region of the samples.

Correlation between H, E, and Y in nanoindentation process

Next, the correlations between H, E, and Y for all of local (at the core region) and global measurements were evaluated at different temperatures and strain rates.

Figure 9(a) shows the correlation between H and E. Least squares straight lines are drawn passing through the origin and the experimental data. The slopes of these lines give the correlational relationships between E and H for the global tensile and local nanoindentation tests, which are 16.28 and 22.12, respectively.

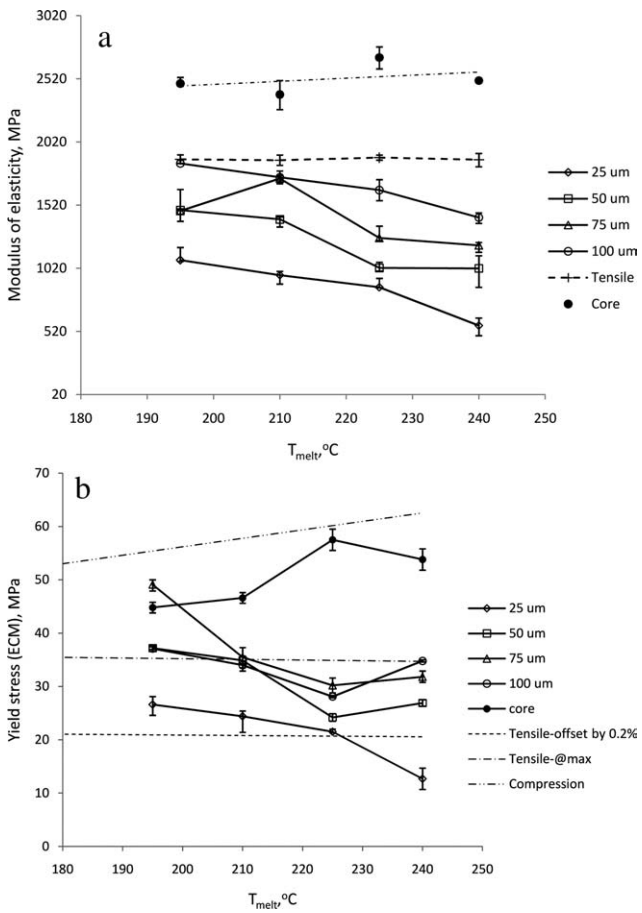

Figure 8 Effect of various melting temperatures (T_{melt}'s) on the local and global scale on the mechanical properties of the iPP samples: (a) E and (b) Y.

TABLE I
Local (Core Region) and Global Mechanical Properties of PP

Test conditions									
Temperature (°C)	Strain rate (1/s)	Melting temperature in injection molding	E_t (MPa)	E_i (MPa)	$Y_t^{0.2}$ (MPa)	Y_t^{max} (MPa)	Y_c (MPa)	Y_{ECM} (MPa)	H (MPa)
20	0.1	240	1880	2506	20	34.8	59.1	53.8	110.7
40	0.1	240	1536	2037	17.1	29.7	51.9	41.5	93.9
60	0.1	240	946	1307	10.6	21.5	38.3	38	79.2
80	0.1	240	586	1115	6.9	15.9	30.1	29	63
20	0.01	240	1745	2500	18	31.8	51.8	49.4	105.3
20	0.001	240	1695	2457	16.4	28.5	49.4	47.5	102.3
20	0.1	225	1897	2689	21.8	34.9	65.6	57.5	121.8
20	0.1	210	1876	2396	20.3	34.9	57.1	46.6	104.1
20	0.1	195	1882	2483	20	35.4	54	44.8	102.3

These results did not agree with those of Flores et al.[18] and Gimenez et al.'s[20] studies. However, nanoindentation results were closer to the work of Gimenez et al. (i.e., $E/H = 20$). Furthermore, as shown in Figure 9(a), the coefficient of correlation, R^2 value for nanoindentation was much higher than that of the tensile test. As shown, the high temperature test data show deviation from straight lines for both nanoindentation and tensile measurements (as indicated by arrows in the figure). This behavior could be explained according to the structural changes occurring during the indentation of semicrystalline polymers. It was stated that the structural changes during indentation could be divided into three steps:[24]

1. Elastic bending of crystals (very small strain),
2. Interlamellar sliding and separation involving shear and compression deformation of amorphous layers (moderate strain), and
3. Lamellar fracture and chain bridging in fractured blocks and destruction of cooperative blocks (large strain).

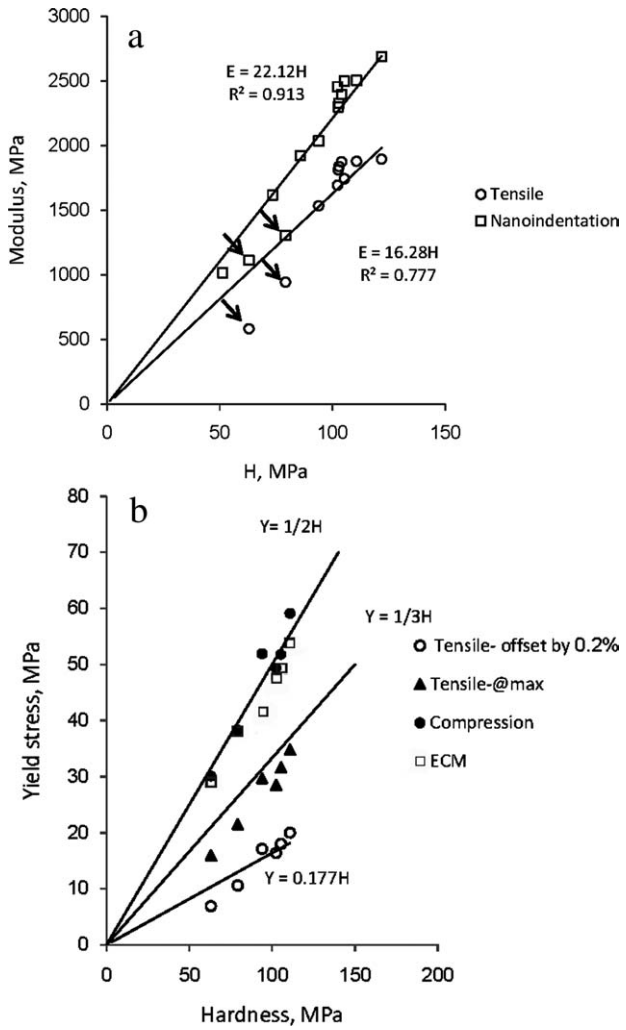

Figure 9 Variation of H with (a) E and (b) Y for different methods of measurement.

Among the aforementioned steps, the elastic bending of crystals, interlamellar sliding, and elastic separation contributed to E_i and E_t at moderate temperatures. However, with increasing temperature, lamellar fracture and chain bridging of the fractured blocks play more important role in the deformation mechanisms of indentation than those of the elastic bending and interlamellar sliding and separation. This means that at moderate temperatures almost the same factors influenced the magnitude of E and H, whereas at elevated temperatures, the elastic part of this

TABLE II
Correlations between *H*, *Y*, and *E* Values for PP

	$c = E/Y$			E/H (measured)		E/H ($= c/b$)	
	E_t	E_i	$b = H/Y$	E_t	E_i	E_t	E_i
$Y_t^{0.2}$	90	120	5.6			16	21.4
Y_t^{max}	50	70	3	16.3	22.1	16.7	23.3
Y_c	30	40	2			15	20
Y_{ECM}	35.2	50	2			17.6	25

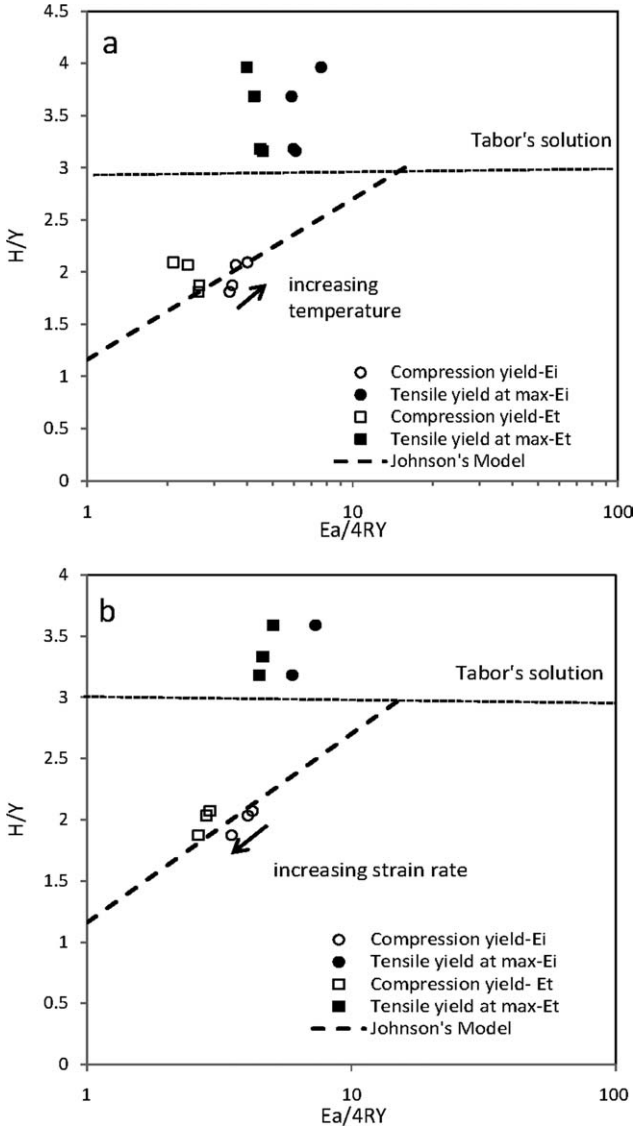

Figure 10 Plots of H/Y versus $\log(E_a/4RY)$ for the local and global measurements at various (a) temperatures and (b) strain rates.

contribution (the first two steps) are diminished. Therefore, the data for high-temperature tests showed deviation from the two straight lines $E_i = 21.1H$ and $E_t = 16.3H$.

Figure 9(b) illustrates the correlation between H and Y, as measured by local and various global methods. As shown, the data from the compression and nanoindentation (ECM) tests were in good agreement with the Flores et al.'s results for compression and microhardness ($H = 2Y_c$) tests. Y_t obtained at a maximum load before the stress-drop was close to but falls slightly below Tabor's solution, that is, $H = 3Y$, and Flores et al.'s tensile experiments. In this case, the deviation of test data from $H = 2Y$ at elevated temperatures was not observed. This means that maybe the same deformation micromechanisms influenced H and Y.

All of the data for the correlation between H, Y, and E are summarized in Table II. The relations (c) between E and Y are also gathered in Table II. We obtained these data by plotting least squares straight lines passing through the origin. E/H values that we obtained by dividing $c = E/Y$ with $b = H/Y$ are also shown in Table II. It is clear that the calculated E/H values agree well with those measured. We concluded that although there was no any agreement between these data and Struik's model, that is, Eq. 9 and Ref [21], a meaningful relation between H, Y, and E was observed.

Evaluation of Johnson's expansion cavity model at different temperatures and strain rates

Figure 10 illustrates the plot of H/Y against $\log(Ea/4RY)$ for the local and global measurements at various temperatures and strain rates. According to Johnson's model, Eq. 6, represented by the dashed straight lines. Tabor's plastic solution, H/Y=3.0, is also superposed as horizontal lines in Figure 10. It can be seen that data points obtained using values of Y_c and E_i follow Johnson's equation. However, with increasing temperature or strain rate, as indicated by arrows in Figure 10, moves towards or away from Tabor's solution. Although the data are few, it can be concluded that the ECM could predict the indentation process at various temperatures and strain rates.

CONCLUSIONS

On the basis of the results obtained, we drew the following conclusions:

- The nanoindentation of PP can be considered a pressure-independent, elastic, perfectly plastic process. For which, Johnson's model is applicable to predict H/Y in the transition region in the indentation process.
- A specific correlation between E_i (obtained at the local core region) and E_t (determined from bulk tensile tests) was found, which is: $E_i = E_t + 500$ MPa.
- The yield stress obtained by nanoindentation, Y_{ECM} is close to the bulk compressive yield stress, Y_c
- The E/H values for the tensile and nanoindentation measurements were found about 16 and 22, respectively. Because at elevated temperatures, the elastic part of deformation beneath the indenter tip was small, this correlation was not valid.
- The relation between H and Y in the compression and nanoindentation tests was found to be

$H \cong 2Y$, different to Tabor's solution. which is followed by the data of H and $Y_t^{\max}$. However, meaningful relations between H, Y, and E was observed.

- With variation of temperature and strain rate, Johnson's model was only valid for Y_{ECM} and the compressive tests as well as E_i.

We would like to thank Prof. Y.-W. Mai and the Australian Research Council for providing financial support to one of us (RLK) for conducting this study at the CAMT, the University of Sydney.

References

1. Tabor, D. Hardness of Metals; Clarendon: Oxford, 1951.
2. Oliver, W. C.; Pharr, G. M. J Mater Res 1992, 7, 1564.
3. Chollacoop, N.; Dao, M.; Suresh, S. Acta Mater 2003, 51, 3713.
4. Cao, Y. P.; Lu, J. Acta Mater 2004, 52, 4023.
5. Lan, H.; Venkatesh, T. A. Acta Mater 2007, 55, 2025.
6. Herbert, E. G. Thin Solid Films 2001, 398–399, 331.
7. Bucaille, J. L.; Stauss, S.; Felder, E.; Michler, J. Acta Mater 2003, 51, 1663.
8. Kramer, D.; Huang, H.; Kriese, M.; Robach, J.; Nelson, J.; Wright, A.; Bahr, D.; Gerberich, W. W. Acta Mater 1999, 47, 333.
9. Sadr, A.; Shimada, Y.; Lu, H.; Tagami, J. Dent Mater 2009, 25, 13.
10. Seltzer, R.; Cisilino, A.; Frontini, P. M.; Mai, Y.-W. Determination of Mechanical Properties of Pressure Sensitive Plastic Solids by Depth Sensing Indentation, submitted to Int J Mech Sci.
11. Briscoe, B. J.; Fiori, L.; Pelillo, E. J Phys D: Appl Phys 1998, 31, 2395.
12. Park, J. M.; Pharr, G. M. Thin Solid Films 2004, 447–448, 246.
13. Johnson, K. L. Contact Mechanics; Cambridge University Press: Cambridge, England, 1985.
14. Hill, R. The Mathematical Theory of Plasticity, Clarendon: Oxford, 1950.
15. Narasimhan, R. Mech Mater 2004, 36, 633.
16. Gao, X. L.; Jing, X. N.; Subhash, G. Int J Solids Struct 2006, 43, 2193.
17. Ai, K.; Dai, L. H. Scr Mater 2007, 56, 761.
18. Flores, A.; Calleja, F. J.; Attenburoow, G. E.; Bassett, D. C. Polymer 2000, 41, 5431.
19. Rueda, D. R.; Viksne, A.; Malers, L.; Balta Calleja, F. J.; Zachmann, H. G. Macromol Chem Phys 1994, 195, 3869.
20. Gimenez, E.; Lagaron, J. M.; Gavara, R.; Saura, J. J. Polym Int 2003, 52, 1243.
21. Struik, L. C. E. J Non-Cryst Solids 1991, 395, 131.
22. Shen, L.; Phang, I. Y.; Liu, T.; Zeng, K. Polymer 2004, 45, 8221.
23. Lesan-Khosh, R. Ph.D. Thesis, Sharif University, 2010.
24. Balta Calleja, F. J.; Fakirov, S. Microhardness of Polymers; Cambridge Solid State Science Series; University of Cambridge: Cambridge, England, 2000.